Journal of Power Sources 196 (2011) 3404–3413

Contents lists available at ScienceDirect

Journal of Power Sources

journal homepage: www.elsevier.com/locate/jpowsour

Development of carbon conductive additives for advanced lithium ion batteries

Michael E. Spahr[a,*], Dietrich Goers[a,1], Antonio Leone[a], Salvatore Stallone[a], Eusebiu Grivei[b]

[a] TIMCAL Ltd., 6743 Bodio TI, Switzerland
[b] TIMCAL Belgium, Appeldonkstraat 168, Willebroek, Belgium

ARTICLE INFO

Article history:
Received 28 March 2010
Received in revised form 20 June 2010
Accepted 1 July 2010
Available online 8 July 2010

Keywords:
Carbon conductive additives
Conductive carbon black
Graphite
Lithium ion batteries
Electrical electrode resistivity
Electrode density

ABSTRACT

The newly developed conductive carbon blacks C-NERGY™ Super C65 and C-NERGY™ Super C45 were studied with regard to their performance as conductive additives in positive lithium ion battery electrodes and compared to other reference conductive carbon blacks. The lowest electrical volume resistivity and highest compressibility were found for C-NERGY™ Super C45 dry-mixed with $LiCoO_2$ powder. Mixing by high shear forces in acetone dispersion improved the electrical resistivity and compressibility of the C-NERGY™ Super C65 containing $LiCoO_2$ mixture to the same level obtained for the C-NERGY™ Super C45 mixture in the same process. Acetone dispersions of C-NERGY™ Super C45 and $LiCoO_2$ showed the lowest viscosities attributed to the carbon black's specific BET surface area of 45 $m^2\ g^{-1}$ being the lowest of all carbon blacks studied. The easy dispersibility of C-NERGY™ Super C45 in $LiCoO_2$ could be explained by its particular surface group chemistry characterized by time-of-flight secondary ion mass spectrometry. The electrical volume resistivity of the $LiCoO_2$/carbon black mixtures was in line with the high current rate performance of half-cells with related $LiCoO_2$ electrodes. Compared to the investigated carbon blacks, the electrical volume resistivity of the graphite conductive additives C-NERGY™ KS6L and C-NERGY™ SFG6L at different concentrations in $LiCoO_2$ powders showed higher critical volume fractions but lower ultimate resistivity levels. Adding one of these graphites to the carbon black conductive mass improved the electrode density and, at concentrations above the critical volume fraction of the graphite component, significantly decreased the ultimate resistivity level of the $LiCoO_2$ electrode mass.

1. Introduction

Over the last two decades lithium ion batteries have become the dominating secondary battery technology in consumer electronics and recently have attracted considerable attention as promising battery technology for emerging automotive and energy storage applications [1–8]. The flexible cell design of the lithium ion battery technology as well as the broad portfolio of existing battery materials allow adapting the cell performance to the battery specifications required for the individual battery type in the small, midsize, and large dimension segment. The electrodes play a key role for the cell characteristics and performance being influenced by the selection of the electrode material types as well as the electrode formulation, design, and engineering [9–12]. The application of a conductive carbon is an important aspect for the electrode engineering even though the conductive carbon is used in the electrode only in small amounts [13,14]. With the nature of the conductive carbon additive, electrode parameters like electrical resistivity, ionic resistivity, and electrode density can be controlled and adjusted. Also parameters of the electrode manufacturing process are affected by the nature of the conductive additive. Particle size and shape are important properties of the electrochemically active electrode material when combining it with the ideal conductive additive [15–19]. In addition, Wang et al. showed that part of the conductive carbon black is incorporated in the polymer binder used in the electrode and that the resulting highly conductive polymer electronically connects the electrode particles [20]. These aspects may explain why a variety of carbon blacks, fine graphites, fibrous products, and nanostructured carbon grades are considered as conductive additives for lithium ion batteries [13,14,21]. At the same time, new conductive carbons optimized in terms of performance, processing, and purity will increase the possibilities for a further improvement of the lithium ion batteries in the portable, automotive and energy storage market segment.

The conductive carbon does not contribute to the electrochemical process of the cell but is required to lower the internal cell resistance and therefore to optimize the power density and specific power of the cell. As the specific energy and energy density of the cell is optimized by keeping the respective amount and volume fraction of conductive carbon as low as possible, there is bound to be a trade-off between cell energy and power. With increasing amount of conductive carbon the electrical electrode resistivity

* Corresponding author. Tel.: +41 91 873 2010; fax: +41 91 873 2019.
E-mail address: m.spahr@ch.timcal.com (M.E. Spahr).
[1] Address: W. Westermann Spezialkondensatoren e.K., Gradestraße 35, 12347 Berlin, Germany.

0378-7753/$ – see front matter © 2010 Elsevier B.V. All rights reserved.
doi:10.1016/j.jpowsour.2010.07.002

decreases by following more or less distinct percolation curves whose shapes depend on both the type of electrochemically active material and the conductive carbon [14,19]. When increasing the volume fraction of the conductive carbon in the electrode, the electrical electrode resistivity remains at a high constant level until the *critical volume fraction* is reached where the electrical resistivity of the electrode sharply drops to a lower resistivity level. At this percolation threshold the conductive paths formed by the conductive carbon through the electrode are completed and the electrode mass percolates to a system of higher conductivity. Further addition of conductive additive does not change the electrode resistivity below the so-called *ultimate resistivity level* which is reached beyond the percolation threshold of the electrical resistivity curve [22]. The critical volume fraction as well as the ultimate resistivity level determines the quality of the conductive additive. With increasing electronic conductivity of the active electrode material the percolation threshold becomes less pronounced.

Besides the critical volume fraction, the surface area and morphology, compaction behavior, as well as the handling and processing of the conductive carbon are important aspects for the electrode engineering. In this paper we describe performance and processing aspects for a family of newly developed conductive carbon blacks and graphite materials. These so-called C-NERGY™ conductive carbons have been recently industrialized and introduced in the lithium ion battery technology. We compare the characteristics of these carbon conductive additives, the effectiveness as conductivity enhancer in the electrode as well as processing aspects relating to reference conductive carbons. In addition, we study the specific role as well as possible positive interactions of graphite and carbon black in conductive masses containing both carbon types, as recently reported by Cheon et al. for a binary conductive carbon system [23]. Performance and processing differences identified between the different carbon types should give instructions for the optimal application of these new carbons and should suggest potential new solutions for the electrode design and engineering targeting the fine-tuning of the performance of lithium ion cells in the different battery application segments.

2. Experimental

2.1. Materials

The graphite materials used throughout this study were fine highly synthetic graphite powders with high degree of crystallinity which were prepared from carbon precursors by an industrial graphitization process based on the Acheson technology and subsequent conditioning [14]. These graphite materials were used as supplied by TIMCAL Ltd. (Switzerland). The C-NERGY™ carbon blacks, Super S®, and Super P® Li supplied by TIMCAL Belgium were produced by converting a hydrocarbon precursor into carbon black in an industrial process based on the partial combustion principle. In this process part of the carbon feedstock is used to generate the energy required for the hydrocarbon cracking and carbon black synthesis according to the following reaction scheme [24]:

$$\text{Combustion}: C_xH_{2x+z} + \left(\frac{3x}{2} + \frac{z}{4}\right) O_2 \rightarrow xCO_2 + \left(x + \frac{z}{2}\right) H_2O + \text{Energy}$$

$$\text{Cracking}: C_xH_{2x+z} + \text{Energy} \rightarrow C_xH_y + \left(x + \frac{z}{2} - \frac{y}{4}\right) H_2 \quad (z > y)$$

$$\text{Synthesis}: C_xH_y \rightarrow xC + \frac{y}{2}H_2$$

In contrast, acetylene black is produced in a special thermal black process based on the exothermic decomposition of acetylene to carbon black and hydrogen above 800 °C [24]:

$$nC_2H_2 \rightarrow 2nC + nH_2$$

The acetylene black powder was used as supplied by Denka Chemicals (Japan). The $LiCoO_2$ had an average particle size distribution of 10 μm and was supplied by Umicore (Belgium).

2.2. Graphite and carbon black material characterization

The oil absorption number (OAN) of carbon black was measured according to ASTM D2414-01 by adding paraffin oil to a carbon black sample by a constant-rate burette. Upon addition of the oil, the free-flowing state of the powder changed to a semi-plastic agglomeration with an accompanying increase of viscosity measured by a torque-sensing system. The OAN was determined from the oil volume measured at a predetermined torque level per carbon mass unit. For the measurement of the absorption stiffness volume (AS) of carbon black, 5 g of carbon black was placed in a 500 mL Erlenmeyer flask. While vigorously shaking the flask with rotating motion, small quantities of a mixture of 10% of acetone in water were added until a stable ball was formed that resisted to fairly shaking without disintegrating. The AS was determined from the quantity of liquid added per 5 g of carbon black. The average aggregate size of carbon black was expressed in terms of the Stokes diameter measured according to DIN EN ISO/IEC 17025. The specific BET surface area (BET SSA) was measured at 77 K in a Micromeritics ASAP2010 nitrogen gas adsorption system. Metal impurities were measured by induced coupled plasma atomic emission spectroscopy (ICP-AES). The carbon samples were burned in a muffle furnace at 800 °C, the ash residue was dissolved in concentrated hydrochloric acid, and the solution was diluted accordingly. The measurement of the pH values for the carbon black samples dispersed in a water/isopropanol (1:1) mixture was measured by a pH electrode. Transmission electron microscopy (TEM) was performed by a JEOL JSM1400. For the sample preparation, the carbons were dispersed in an isopropanol/water mixture by an ultrasonic bath, the liquid dispersion was put on the sample holder and the solvent subsequently was evaporated.

The graphite real density was measured in terms of xylene density with the help of a pycnometer according to DIN 51 901, the apparent density of graphite in terms of Scott density in a Scott apparatus according to ASTM B 329-98 2003. The graphite particle size distribution was measured by laser diffraction using a MALVERN Mastersizer S. The graphite oil absorption was measured according to ASTM D2414 05a by covering 0.5 g of graphite with 1.5 g of Marcol 82 paraffin oil (Exxon, USA). The oil graphite mixture was centrifuged at $512 \times g$ ($1\,g = 9.81\,m\,s^{-1}$) in a metal centrifuge tube equipped with a filter paper which was wetted by paraffin oil centrifuged at $512 \times g$ prior to its use. The oil absorption per 100 g graphite was calculated from the weight increase of the dry and the graphite sample after centrifugation.

Time-of-flight secondary ion mass spectrometry (TOF-SIMS) measurements were performed with a PHI-Evans TFS-4000MMI (TRIFT) spectrometer as described in more details elsewhere [25]. The sample was bombarded with a pulsed $^{69}Ga^+$ ion beam (15 keV, 800 pA d.c., 11 kHz frequency and 20 ns unbunched pulse width). The secondary ions were accelerated to ±3 keV by applying a bias on the sample. The initial kinetic energy spreading of the secondary ions was compensated by a 270° deflection in three electrostatic analyzers. To increase the detection efficiency of high mass-ions, a 10 keV post-acceleration was applied at the detector entry. The analyzed area was a square of 130 μm × 130 μm. The TOF-SIMS positive mass spectrum was recorded in a m/z range of 0–600, the

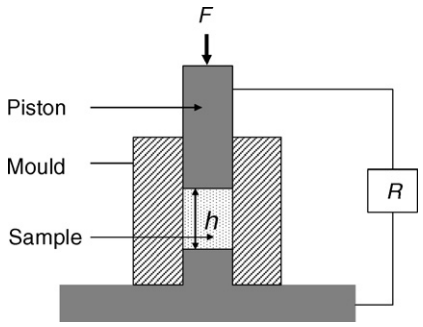

Fig. 1. Schematic drawing of the experimental set-up used for the two point electrical resistivity measurement; *F* is the force applied to compress the powder sample to the height *h* at which the measurement of the electrical volume resistance *R* is performed.

TOF-SIMS negative mass spectrum in a *m*/*z* range between 10 and 100.

2.3. Electrical resistivity and electrochemical measurements

Dry blends of $LiCoO_2$ and conductive carbon were prepared in a Turbula mixer by mixing 10 g of sample for 60 min. The wet blending was achieved by first dispersing carbon black in acetone with the help of a high shear energy laboratory mixer Ultra Turrax® T25 basic (IKA Labortechnik, Switzerland) and subsequently mixing the $LiCoO_2$ into the suspension. The suspensions were dried at 100 °C to isolate the powder mixture. The electrical volume resistivity and compaction measurement of the powder samples were performed in the 2-electrode set-up schematically illustrated in Fig. 1. The experiments were performed at room temperature by increasing the pressure from 50 to 450 kg cm^{-2} in pressure increments of 50 kg cm^{-2}. Samples having a mass of several grams were mounted into an electrically insulating mould with an internal cross-section of 1.33 cm^3. The bottom of the mould as well as the piston was copper-made and electrically connected to a Keithley 2000 digital multimeter in order to measure the electrical resistance of the sample. The electrical volume resistivity σ of the powder samples was calculated from the electrical resistance *R* measured between the two electrodes with an area of 1.33 cm^2 and the sample height *h* according to:

$$\sigma = R\frac{A}{h} \quad (1)$$

Both the height and the electrical resistance of the samples were measured at a given pressure after waiting for about 30 s to stabilize the sample. The sample density ρ was calculated from the sample weight *m* and sample volume *Ah* according to:

$$\rho = \frac{m}{Ah} \quad (2)$$

The mechanical energy, E_i, which is required to compact the powder sample to a sample density ρ was calculated from the changes of the sample height, h_j, and the corresponding pressure, p_j, applied between the two electrodes:

$$E_i = \sum_{j=1}^{i} p_j A(h_{j-1} - h_j) \quad (3)$$

Electrochemical measurements were performed at 25 °C in a gas-tight, coin-cell-like arrangement using a computer controlled cell capture system (CCCC, Astrol Electronic AG, Switzerland) [26]. Electrodes were prepared by blade-coating a dispersion of 94 wt.% of $LiCoO_2$, 3 wt.% of conductive carbon, and 3 wt.% KF Polymer L #9130 polyvinylidene difluoride (PVDF) (Kureha Chemical Co., Japan) in N-methyl pyrolidone (NMP) on an aluminum foil current collector. The rheology of the dispersions was measured by a Physica MCR300 Rheometer (Paar Physica, Germany) at shear rates ranging from 0.001 to 1000 s^{-1}. The electrodes were dried at 100 °C. The electrodes had a geometric area of 1.33 cm^2 and a mass loading of 30 mg cm^{-2}. The electrodes were pressed to a final density of 3.50 ± 0.03 g cm^{-3}. Metallic lithium (0.75 mm thick foil, Alfa Aesar, Johnson Matthey GmbH, Germany) served both as the reference and counter electrode. 1 M $LiPF_6$ dissolved in ethylene carbonate/diethyl carbonate (1:3, by volume) was used as electrolyte (Ube Industries Corp., Japan). The water impurities of the commercial electrolytes were analyzed by Karl–Fischer titration and always were found to be below 10 ppm. A 1 mm thick soft glass–fiber sheet (Hollingsworth & Vose, Ltd.) was used as separator. The electrode as well as the glass–fiber separator were dried at 120 °C at a reduced argon pressure of 10^{-3} mbar for 12 h and then stored in a dry argon atmosphere prior to the cell assembly. The cell assembly was performed in a glove box having an argon atmosphere with a humidity level below 1 ppm. The double layer capacitance was calculated from the impedance of the half-cell at 10 mHz and 2.5 V versus Li/Li$^+$ using a SI1260 Impedance Analyzer connected to a SI1287 Electrochemical Interface (Solartron Analytical, France).

3. Results and discussion

Usually carbon black grades used as conductive carbon in lithium ion batteries belong to the family of conductive carbon blacks. Characteristic feature of conductive carbon blacks is the large complex carbon black structure of the primary carbon black particles forming chemically bound aggregates that tend to further agglomerate [22]. The complexity of the arrangements of the carbon black primary particles and the carbon black aggregates in the agglomerated aggregates results in void volumes in the interstices of the carbon black aggregates and the inter-aggregate space. The void volume is used as a measure to compare the structure of carbon blacks. The void volume depends on the size and shape of the aggregates, the aggregate agglomerates, and the porosity of the primary particles. The higher the structure level of the aggregate is, the higher is the volume of the voids. The oil absorption number, OAN, as well as the absorption stiffness volume, AS, are employed to measure the void volume and thus the average structure level. The higher the OAN and AS are, the more complex is the structure of the aggregates. An OAN of 170 mL (100 g)$^{-1}$ carbon is given as lower limit for the family of conductive carbon blacks. Since the carbon black structure is the prerequisite to form and maintain a carbon network in the electrodes mass [27] the OAN and AS can be considered as first indicators for the performance of a carbon black as conductive additive. Recent investigations have shown that the evolution of the volume of a given carbon black weight under increasing pressure as well as the electrical resistivity at low carbon black densities is another way to describe the carbon black structure and therefore to categorize carbon blacks. Conductive carbon blacks show high volumes at low pressures as well as low intrinsic electrical resistivities at low compressed densities [28,29]. Acetylene black, special furnace blacks, gasification black like Ketjen black as well as Super S® and Super P® Li are known as carbon black grades with high carbon black structure.

As reference conductive carbon blacks in our investigation, we selected grades with a BET SSA below 100 m^2 g^{-1}: acetylene black, Super S® and Super P® Li. Fig. 2 shows the electrical resistivity as a function of the sample density of pure $LiCoO_2$ as well as of dry blends containing $LiCoO_2$ and 3 wt.% conductive carbon black. The sample density was calculated for each pressure applied to the powder sample between the two electrodes. As in all experiments

Table 1
Key properties of the investigated conductive carbon black grades.

Carbon black	BET SSA ($m^2\,g^{-1}$)	Stokes diameter DIN EN ISO/IEC 17025 (nm)	Absorption stiffness (AS) ($mL\,(5\,g)^{-1}$)
Acetylene black	72	159	34
Super P® Li	62	144	32
Super S®	50	178	34
C-NERGY™ Super C65	62	150	32
C-NERGY™ Super C45	45	209	37

the pressure was increased from 50 to 450 kg cm^{-2} according to the same stepwise protocol of using 50 kg cm^{-2} pressure increments, the *n*th measurement point of each curve corresponds to the same applied pressure value and therefore can be considered as isostatic point. The electrical resistivity at the highest density of every curve was measured at 450 kg cm^{-2} being the highest possible pressure of the experimental set-up. Typically, the electrical resistivity decreased with increasing sample density and corresponding pressure due to an improving electrical interparticle contact or due to the decreasing distance of the carbon black aggregates if an electron hopping or tunneling mechanism is assumed as conduction mechanism in the conduction pathways. In addition, with the increasing pressure between the sensing electrodes, the contact resistance at the electrodes of the two point measurement system contributing to the total electrical resistance decreased. Pure $LiCoO_2$ powder showed an electrical resistivity of about 2.6 kΩ cm at a corresponding sample density of 3.6 g cm^{-3} and pressure of 450 kg cm^{-2}. Note that the theoretical density of the $LiCoO_2$ is 5.2 g cm^{-3}. The lower electrical resistivities of more than one order of magnitude obtained for the carbon black containing samples compared to the pure $LiCoO_2$ indicated the conductivity enhancing effect of the carbon blacks. At the same time with the addition of carbon black to the $LiCoO_2$ the sample densities significantly decreased. These decreased sample densities could be explained by the low volume density and low compressibility of carbon black. Significant differences in electrical resistivity were observed between the carbon black grades. The electrical volume resistivity of $LiCoO_2$ containing 3 wt.% carbon black varied over more than one order of magnitude and decreased in the order Super S®, acetylene black, and Super P® Li.

The C-NERGY™ conductive carbon blacks were developed by screening the process parameters of a new industrial manufacturing process recently designed with strict impurity control. Carbon black products found in this screening process with the lowest volume electrical resistivities in standard positive electrode materials were industrialized. Typical iron impurities for carbon black products generated in this new manufacturing process were found to be below 2 ppm. Table 1 compares the key carbon black properties of the newly developed industrial products, C-NERGY™ Super C65 and C-NERGY™ Super C45, with the reference carbon blacks. C-NERGY™ Super C65 showed similar BET SSA as Super P® Li. The average aggregate size measured according to Stokes and the absorption stiffness indicated similar carbon black structures. Compared to these carbon blacks, C-NERGY™ Super C45 showed a significantly lower BET SSA; the increased Stokes diameter and AS indicated a slightly larger carbon black structure. C-NERGY™ Super C45 shows a similar BET SSA as Super S® but a slightly larger carbon black structure.

TEM images of C-NERGY™ Super C65 and C-NERGY™ Super C45 shown in Fig. 3 indicate the large carbon black structure of both carbon blacks and, in the case of C-NERGY™ Super C45, slightly larger primary particles. As for carbon blacks with a BET SSA below

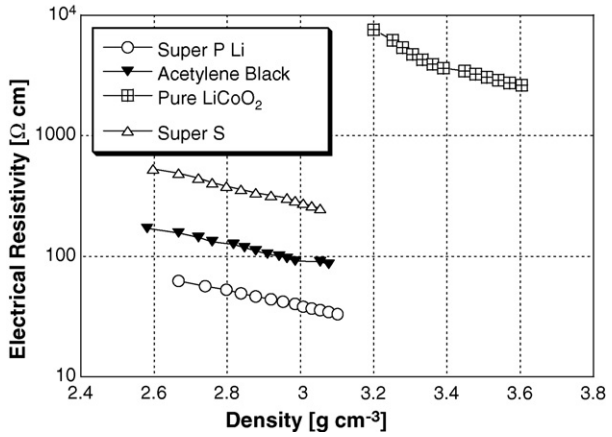

Fig. 2. Electrical volume resistivity versus density of powder samples consisting of pure $LiCoO_2$ and $LiCoO_2$ dry-mixed with 3 wt.% of either acetylene black, Super P® Li, and Super S® conductive carbon blacks.

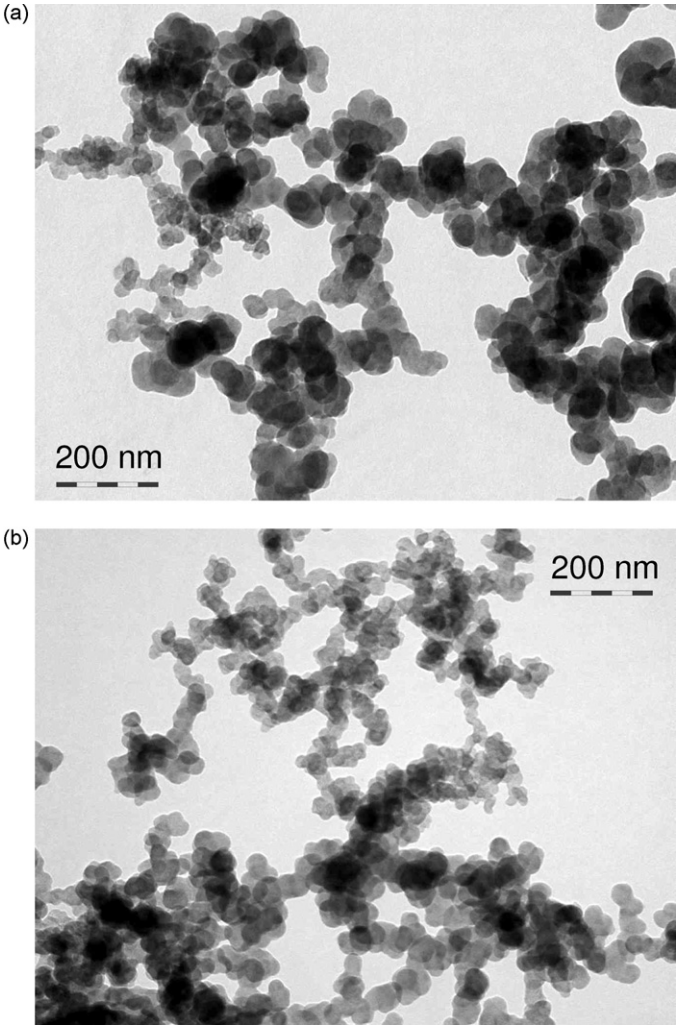

Fig. 3. TEM images of C-NERGY™ Super C45 (a) and C-NERGY™ Super C65 (b) conductive carbon blacks.

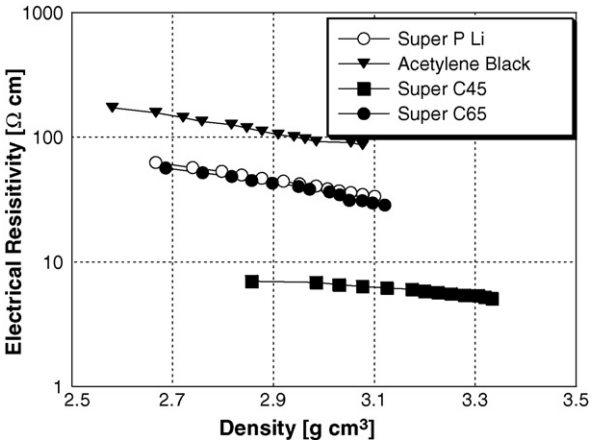

Fig. 4. Electrical volume resistivity as a function of the density of powder samples consisting of $LiCoO_2$ dry-mixed with 3 wt.% of either acetylene black, C-NERGY™ Super C45, or C-NERGY™ Super C65 conductive carbon blacks.

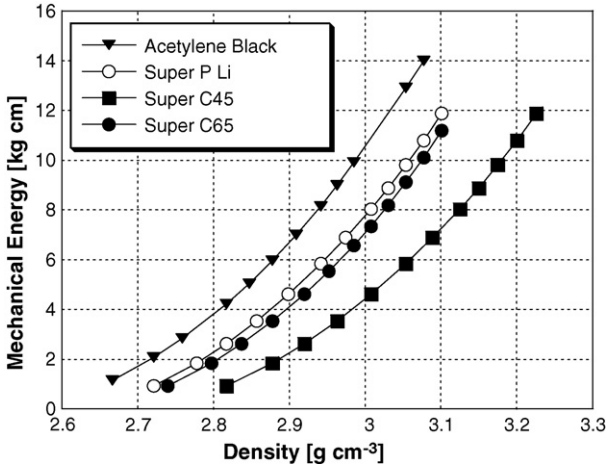

Fig. 5. Mechanical energy required to compress powder samples of $LiCoO_2$ dry-mixed with 3 wt.% of acetylene black, C-NERGY™ Super C45, or C-NERGY™ Super C65 conductive carbon blacks.

$100\,m^2\,g^{-1}$ no significant porosity can be expected, it is mainly the geometrical surface area of the carbon black that in the case of such carbon blacks contributes to the surface area. The specific surface area as determined by the electron microscope (EMSA) can directly be derived from the surface mean diameter d_{sm} (in nm) and the carbon black density ρ, according to the following expression [27]:

$$S\,(m^2\,g^{-1}) = \frac{6000}{\rho d_{sm}} \tag{4}$$

Statistical image analysis of a selection of TEM pictures resulted in arithmetic mean primary particle diameters of 37 and 32 nm for C-NERGY™ Super C45 and C-NERGY™ Super C65, respectively based on the evaluation of about 2000 primary particles. In the case of C-NERGY™ Super C45, we calculated an EMSA of $67\,m^2\,g^{-1}$ from a carbon black density of $\rho = 1.86\,g\,cm^{-3}$ and a surface mean diameter of 48 nm determined by the statistical image analysis. In the case of C-NERGY™ Super C65, a surface mean diameter of 37 nm and the same density resulted in an EMSA of $87\,m^2\,g^{-1}$. The difference between the arithmetic mean and surface mean diameter is a fingerprint for polydispersity. The lower BET SSA of C-NERGY™ Super C45, compared to C-NERGY™ Super C65, hence, can be explained by the larger size of its primary particles.

Fig. 4 shows the electrical volume resistivity of the two C-NERGY™ carbon blacks in comparison to the reference carbon blacks. Compared to Super P® Li, C-NERGY™ Super C65 showed in $LiCoO_2$ quasi identical resistivity values which, due to the similar carbon black structure, could be expected. Interestingly, C-NERGY™ Super C45 containing $LiCoO_2$ mixtures showed a significantly decreased electrical resistivity and higher sample density compared to Super P® Li and acetylene black. The improved compaction behavior of C-NERGY™ Super C45 containing $LiCoO_2$ mixtures can be presented in a different angle by plotting the mechanical energy calculated according to Eq. (3) against the corresponding sample densities. The resulting curves are shown in Fig. 5. The mechanical energy required to compact the powder mixture to the corresponding sample density was the lowest for C-NERGY™ Super C45. As the density values for the carbon black containing mixtures range significantly below the values obtained for the pure $LiCoO_2$, it is presumably the carbon black component which controls the compaction behavior of the powder mixtures. The shape of the energy curves further verifies this assumption. It is well accepted in the carbon black literature that the mechanical properties of carbon blacks are mainly governed by the electrical state, i.e. that the strength of the carbon black agglomerates and the breakdown of the carbon black structure are controlled by electrical surface charges [28,29]. Following this approach, electrostatic repulsion forces of these electrical surface charges would be responsible for the mechanical energy required to compact the $LiCoO_2$ mixtures. The work achieved against these repulsion forces depends on the sum of the electrical surface charges q_i and q_j at a distance $r_{i,j}$:

$$E \propto \sum_{i,j} \frac{q_i q_j}{r_{i,j}} \tag{5}$$

With decreasing distance $r_{i,j}$ during the compaction of the powder samples, the repulsive energy exponentially increases which could explain the compaction behavior observed for the sample mixtures. Moreover the lower mechanical energies found in the case of the C-NERGY™ Super C45 mixture would indicate either less electrical surface charges or a lower amount of agglomerates, i.e. a better dispersion of the C-NERGY™ Super C45 in the $LiCoO_2$.

To verify this assumption, we compared the electrical volume resistivity of the dry-blended carbon black/$LiCoO_2$ mixture with a powder sample taken from a liquid mixing process in which the carbon black was dispersed in acetone with a high shear force mixer prior to the $LiCoO_2$ was mixed into the carbon black suspension. The electrical resistivity curves of the powder samples prepared in the dry and wet-mixing process are shown in Fig. 6. Whereas the electrical resistivity of the C-NERGY™ Super C65 containing mixture significantly decreased by the high shear mixing in acetone, the resistivity of the C-NERGY™ Super C45 slightly increased under such wet-mixing conditions. Apparently, the agglomerates of C-NERGY™ Super C65 could more efficiently be broken by the high shear mixing in liquid medium leading to a more homogeneous dispersion of the carbon black aggregates in the powder mix. In contrast, the agglomerates of C-NERGY™ Super C45 are less stable and were efficiently dispersed by the more gentle dry-mixing process. Under the influence of high shear energy applied in the liquid process, the C-NERGY™ Super C45 aggregates slightly degraded as it was indicated by the increased electrical resistivity. These results indicate that for an optimal electrode performance, not only the selection of the carbon black but also the adaptation of the mixing process is important.

To better understand the different behavior of C-NERGY™ Super C65 and C-NERGY™ Super C45 in terms of dispersibility and miscibility, we analyzed the surface group chemistry by TOF-SIMS. Super S® was included in the study as a reference carbon having a similar BET SSA as C-NERGY™ Super C45. The evaluation and comparison of the positive TOF-SIMS spectra indicated significant intensity

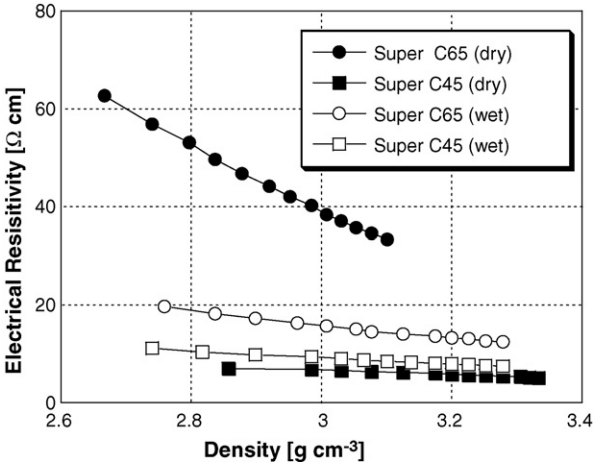

Fig. 6. Comparison of the electrical resistivity at corresponding densities of samples prepared by either dry-mixing or wet-mixing under the influence of high shear energy. The subsequently dried samples consisted of $LiCoO_2$ and 3 wt.% of either C-NERGY™ Super C45 or C-NERGY™ Super C65 conductive carbon black.

differences of mass signals assigned to hydrocarbon cluster ions $C_xH_y^+$ with an aromatic structure as well as to protons, and to oxygenated hydrocarbon ions $C_xH_yO^+$. The negative TOF-SIMS spectra showed remarkable differences in the mass signal assigned to carboxylic acid $COOH^-$. The results of the TOF-SIMS investigations are summarized in Fig. 7. The relative intensity of the mass signals assigned to aromatic hydrocarbons was significantly lower for C-NERGY™ Super C45 than for C-NERGY™ Super C65 and Super S®. This indicated a lower degree of graphitization and sp^2 carbon concentration at the primary particle surface of the first carbon black. The significantly higher relative intensity of the hydrogen mass signals found for C-NERGY™ Super C45 was in line with the previous results about the aromatic clusters and confirmed the decreased surface aromaticity of this carbon black. A higher relative intensity of the mass signals assigned to oxygenated hydrocarbons was attributed to a higher concentration of oxide groups at the surface of C-NERGY™ Super C45. In addition, a significantly higher intensity of the mass signals assigned to carboxylic acid surface functional groups was found for this carbon black. Similar relative mass peak intensities for aromatic carbon, hydrogen, oxide, and carboxylic acid surface groups were observed for C-NERGY™ Super C65 and

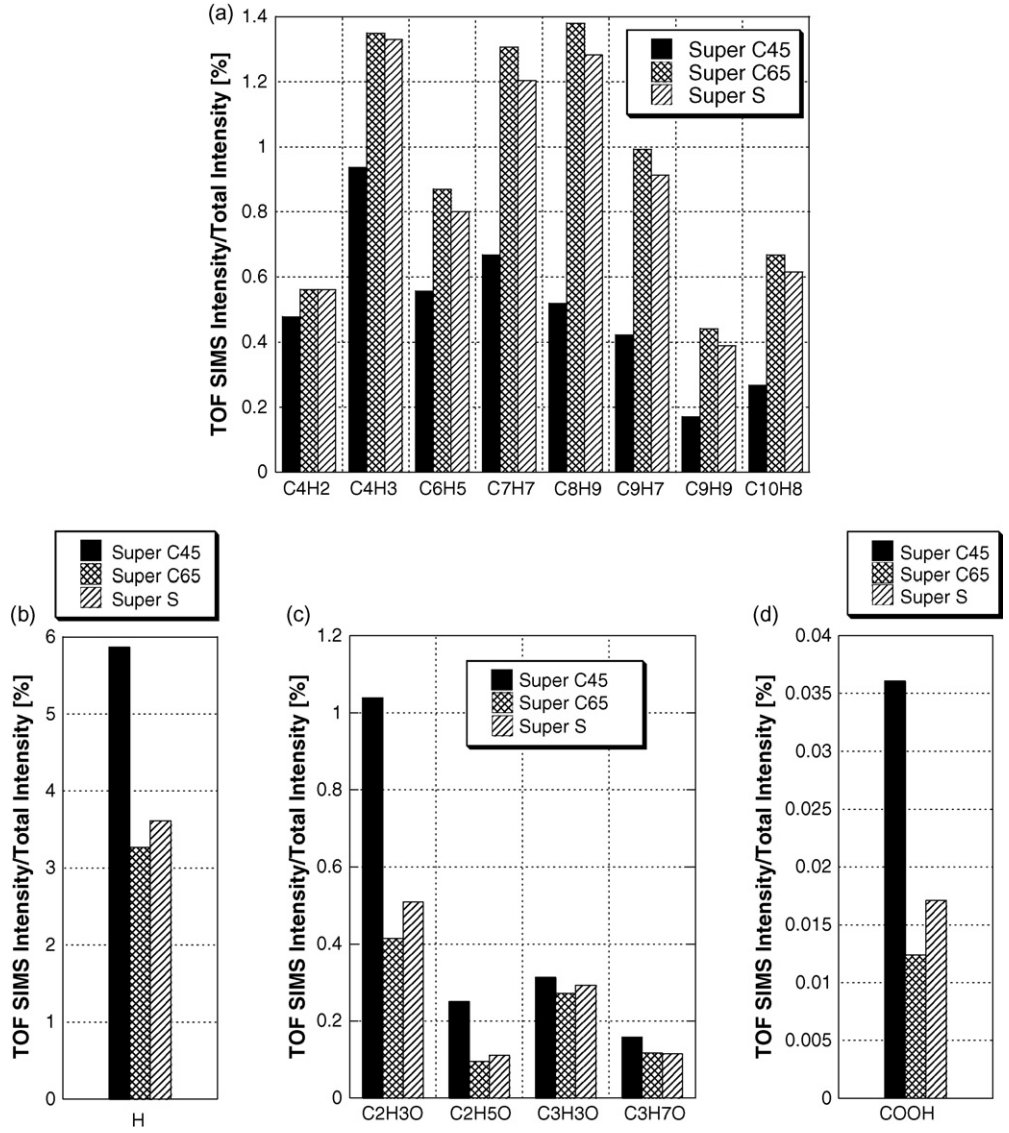

Fig. 7. Relative intensities of mass signals observed in TOF-SIMS measurements of C-NERGY™ Super C45, C-NERGY™ Super C65, and Super S® conductive carbon black. The intensity of mass signals assigned to aromatic carbon (a), oxygen groups (b), and hydrogen groups (c) were observed in the positive mass signal spectrum. The intensity of mass signals assigned to carboxylic acid groups was observed in the negative mass signal spectrum.

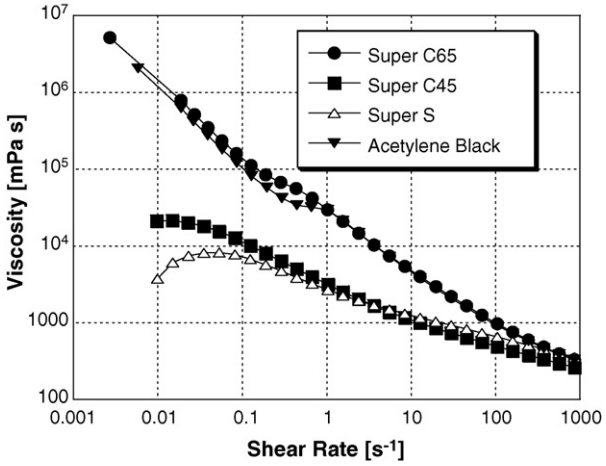

Fig. 8. Rheology of 94 wt.% of $LiCoO_2$, 3 wt.% PVDF, and 3 wt.% of either C-NERGY™ Super C45, C-NERGY™ Super C65, Super S®, or acetylene black dispersed in N-methyl pyrolidone for the same total mass of the dispersion.

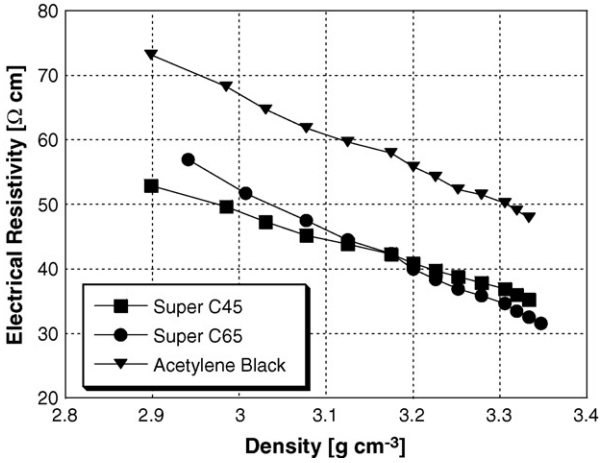

Fig. 9. Electrical resistivity as a function of the density of dried powder samples consisting of $LiCoO_2$ and 2 wt.% different conductive carbon blacks mixed in acetone with high shear energy.

Super S® indicating the same or similar surface group chemistry and aromaticity at the particle surface. The increased concentration of surface oxide and carboxylic acid functional groups is reflected in the lower pH value of C-NERGY™ Super C45 in aqueous media (pH 7) compared to C-NERGY™ Super C65 and Super S® (both pH 10).

The rheology of carbon black containing dispersions is an important parameter for the electrode manufacturing if it is based on a liquid coating process. Fig. 8 shows the rheology of NMP dispersions of 3 wt.% of carbon black, 94 wt.% of $LiCoO_2$, and 3 wt.% of PVDF with formulations based on the same total dispersion amount. For each of these dispersions the carbon black agglomerates were predispersed by high shear mixing in a solution of PVDF in NMP prior to the addition of the $LiCoO_2$. The obtained flow curves were similar for the C-NERGY™ Super C45 and Super S® dispersions. However, for both carbon blacks, the viscosities of the NMP dispersions at corresponding shear rates applied in the rheology measurement were significantly lower than in the case of C-NERGY™ Super C65 and acetylene black. These results indicated that, provided that the agglomerates of the carbon blacks are ideally dispersed in the solvent medium and the aggregates are isolated and stabilized against coagulation, it is neither the surface group chemistry nor the structure of the carbon black, but solely the BET SSA which controls the rheology of the carbon black containing liquid dispersion.

Due to the influence of the carbon black dispersibility and sample preparation on the electrical resistivity results, we used for the following investigations exclusively the sample preparation based on the wet-mixing process. When lowering the carbon content from 3 to 2 wt.%, similar electrical volume resistivities were obtained for the two C-NERGY™ carbon blacks, as shown in Fig. 9. Fig. 10 shows the variation of the electrical volume resistivity at different carbon black amounts for mixtures of $LiCoO_2$ with C-NERGY™ Super C65, C-NERGY™ Super C45 or acetylene black. In the concentration range between 1 and 5 wt.% of carbon, the electrical volume resistivity was similar for two C-NERGY™ carbon blacks. The critical carbon black amount, at which the percolation threshold was observed, was similar for the C-NERGY™ carbon blacks but slightly lower for acetylene black. However, compared to acetylene black, the two C-NERGY™ carbon blacks showed lower ultimate resistivity levels in $LiCoO_2$ mixtures.

To correlate the electrical resistivity measurements with the high current drain performance at cell level, we prepared $LiCoO_2$ electrodes containing C-NERGY™ Super C45, C-NERGY™ Super C65, Super S®, or acetylene black and tested them in lithium half-cells. Fig. 11 shows for subsequent charge/discharge cycles the specific charge which was obtained for the galvanostatic charging process of the half-cell at C/2 in relation to the specific charge obtained galvanostatically during cell discharge in the same cycle. The fading of the specific charge retention during cycling could be attributed to the lithium negative electrode. The relative galvanostatic specific charge was similar for the two C-NERGY™ carbon black containing electrodes and during cycling remained at a higher level than for the acetylene black and Super S® containing $LiCoO_2$ electrodes. The similar electrical volume resistivities observed in the case of the two C-NERGY™ carbon blacks in $LiCoO_2$ powder mixtures as well as the ranking of the studied carbon blacks with regard to the electrical volume resistivity of their $LiCoO_2$ mixtures correlated with the high current drain charging performance of half-cells containing the related positive electrodes. To compare the electrode surface area which is wetted by the liquid electrolyte, we performed impedance spectroscopy of the lithium half-cells prior to the first charge/discharge cycle. We calculated the double layer capacitance of the electrodes from the impedance measured at 10 mHz and 2.5 V versus Li/Li^+. The lowest double layer capacitance was found for the C-NERGY™ Super C45 containing $LiCoO_2$ electrode indicating the lowest wetted electrode surface area presumably due to the low BET SSA of the carbon black (Fig. 12). This

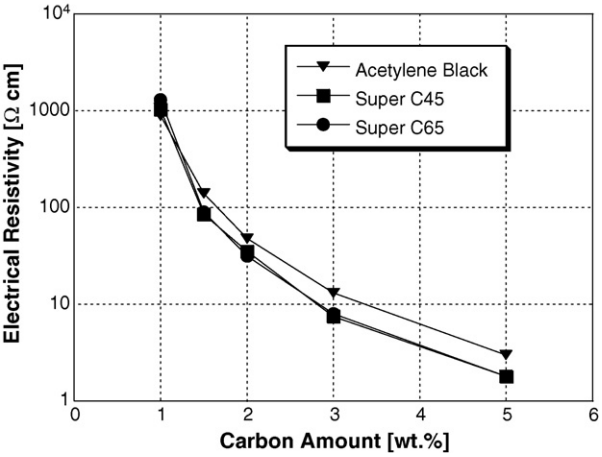

Fig. 10. Electrical volume resistivity measured at 450 kg cm^{-2} and different carbon amounts for dried powder mixtures of $LiCoO_2$ and C-NERGY™ Super C45, C-NERGY™ Super C65, or acetylene black wet-mixed in acetone dispersion with high shear energy.

Table 2
Material properties of the investigated graphite conductive additives.

Material parameters	Average particle size (μm)	Scott density (g cm^{-3})	Xylene density (g cm^{-3})	BET SSA (m^2 g^{-1})	Oil absorption (mL (100 g)$^{-1}$)
TIMREX® KS6	3.4	0.07	2.25	20	150
C-NERGY™ KS6L	3.2	0.06	2.25	20	155
C-NERGY™ SFG6L	3.6	0.05	2.25	17	165

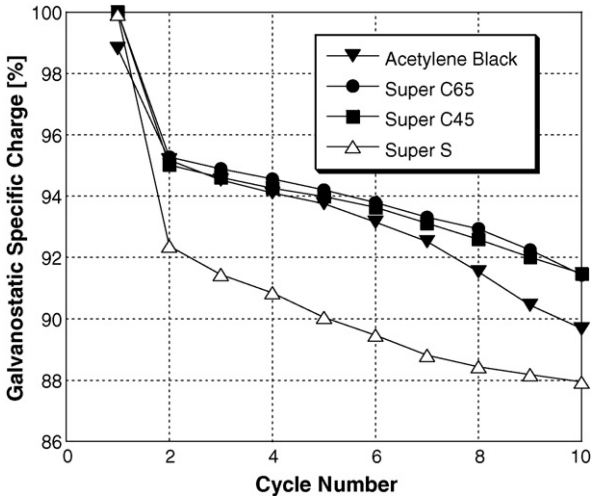

Fig. 11. Specific charge of a lithium half-cell containing $LiCoO_2$ and 3 wt.% of either C-NERGY™ Super C45, C-NERGY™ Super C65, Super S®, or acetylene black obtained by galvanostatic charging at C/2.

is remarkable in view of the performance of this electrode in the high rate charging tests described above. In addition, a lower reaction rate for chemical and electrochemical side reactions could be expected for the lower wetted electrode surface area which could be an advantage for the cycling stability and durability of the cell containing C-NERGY™ Super C45.

Fine graphite powder is used as an alternative to carbon black conductive additives in lithium ion battery electrodes. Graphite significantly varies from conductive carbon black in morphology, crystallinity, texture, density, particle size, and surface properties. Table 2 summarizes the material properties of the fine graphite products TIMREX® KS6, C-NERGY™ KS6L, and C-NERGY™ SFG6L used in this study. All three grades show a similar particle size distribution with an average particle size of about 3 μm. In the order KS6-KS6L-SFG6L the volume density given in terms of Scott density slightly decreases whereas the oil absorption increases which indicate a slightly increasing anisometry of the particle shape in this order. Fig. 13 shows TEM pictures of a C-NERGY™ SFG6L and C-NERGY™ KS6L graphite particle. These TEM pictures illustrate the specific features of the graphite texture and particle mosaicity. A graphite particle cannot be considered as one single crystal but has polycrystalline morphology. SFG6L particles contain a few rather large single crystal domains which are oriented parallel to the particle platelet plane as it is indicated by the shaded areas of the TEM image in Fig. 13a. In contrast, KS6L contains a larger number of smaller single crystals which are more or less randomly oriented in the particle giving rise to more isotropic behavior of the graphite properties (Fig. 13b). The existence of single crystal domains in the graphite particles being more than 10-fold larger in dimension is a striking difference of graphite in comparison to conductive carbon black. This morphological difference presumably causes different conduction mechanisms for both types of conductive additives. In

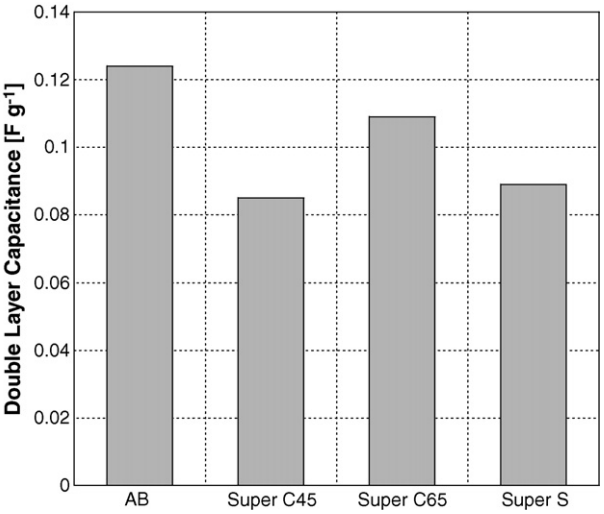

Fig. 12. Double layer capacitance calculated from the impedance at 10 mHz of a lithium half-cell containing $LiCoO_2$ and 3 wt.% of either C-NERGY™ Super C45, C-NERGY™ Super C65, Super S®, or acetylene black (AB).

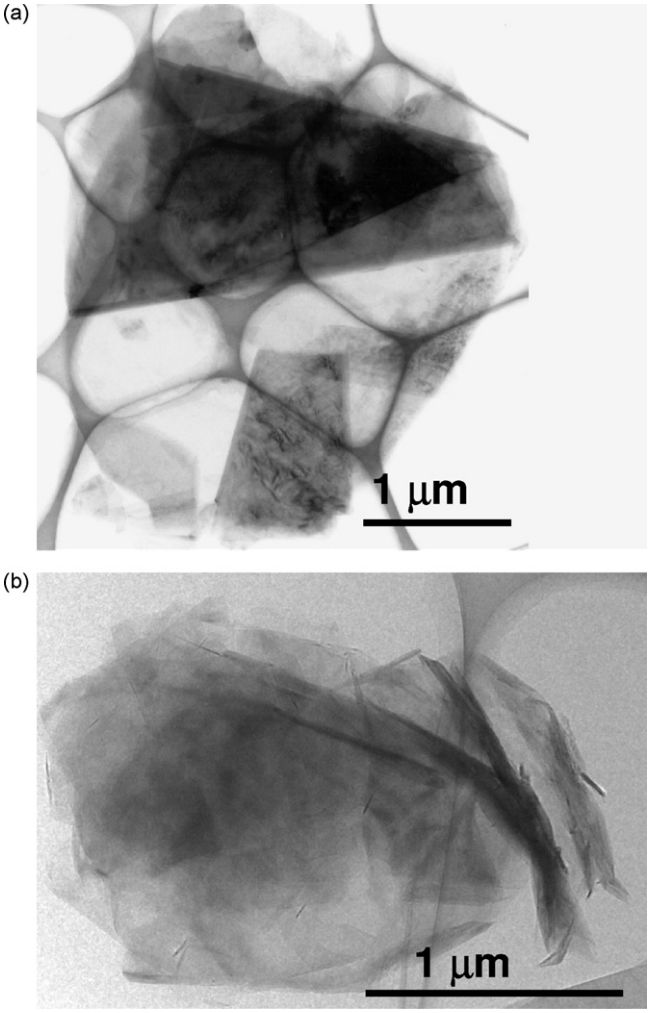

Fig. 13. TEM images of TIMREX® SFG6L (a) and TIMREX® KS6L (b).

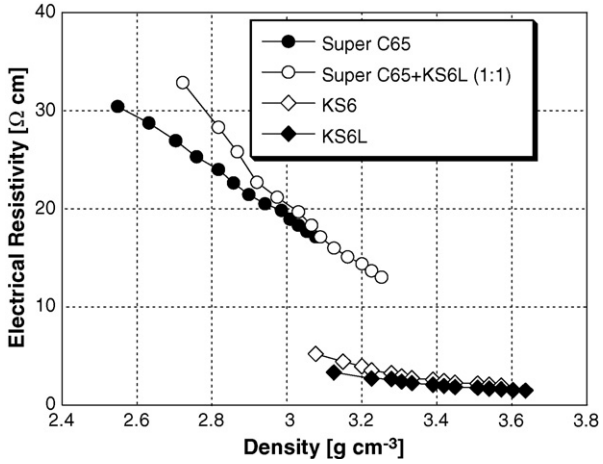

Fig. 14. Electrical volume resistivity versus sample density of dried powder samples consisting of $LiCoO_2$ and 5 wt.% of total carbon conductive mass mixed in acetone with high shear energy. The conductive additives shown are C-NERGY™ KS6L or TIMREX® KS6 graphite, C-NERGY™ Super C65 carbon black as well as a blend of C-NERGY™ Super C65 and C-NERGY™ KS6L (1:1 by weight).

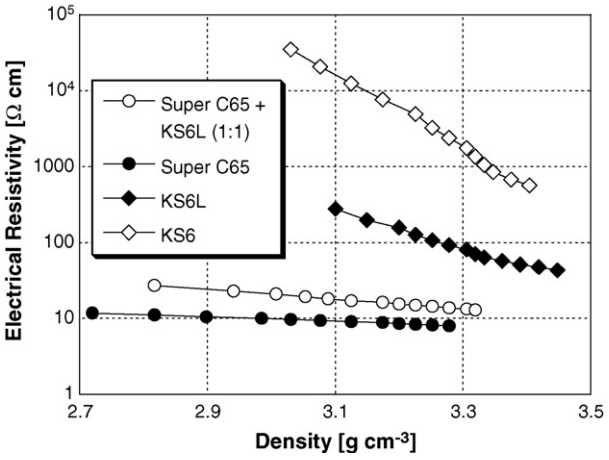

Fig. 15. Electrical volume resistivity versus sample density of dried powder samples consisting of $LiCoO_2$ and 3 wt.% of total carbon conductive mass mixed in acetone with high shear energy. Conductive additives were C-NERGY™ KS6L or TIMREX® KS6 graphite, C-NERGY™ Super C65 carbon black as well as a blend of C-NERGY™ Super C65 and C-NERGY™ KS6L (1:1 by weight).

addition, a significantly lower BET SSA and oil absorption of fine graphite compared to conductive carbon black influence the electrode design and manufacturing process parameters like the lower required binder amount as well as the lower dispersion viscosity which are expected for graphite containing electrodes.

Fig. 14 compares the electrical volume resistivity of $LiCoO_2$ powder samples containing graphite, carbon black, and mixtures thereof as a function of the compressed density at a carbon content of 5 wt.% carbon which is far beyond the critical volume fraction of both graphite and carbon black grades. At this concentration in the low resistivity domain of the percolation curves, significantly lower electrical volume resistivities were obtained for the graphite containing samples: $LiCoO_2$ samples containing either KS6 or KS6L graphite at 5 wt.% showed similar electrical resistivities that were significantly lower than the values found in the case of C-NERGY™ Super C65. The higher apparent density and compressibility of graphite could be responsible for the significantly higher sample densities obtained for the graphite containing powders. These higher sample densities could cause an improved direct particle contact between the graphite particles as well as between the graphite and $LiCoO_2$ particles which could explain the lower resistivity values found for graphite containing samples. Apparently, the ultimate resistivity level in the percolation curves of the $LiCoO_2$/carbon mixtures is lower for the KS6 and KS6L graphite than for the C-NERGY™ carbon black grades. When adding KS6L graphite to the C-NERGY™ Super C65 carbon black conductive mass, the sample densities increased due to the higher compressibility and volumetric density of graphite compared to carbon black. The higher densities could explain the lower electrical resistivities obtained at high concentration of the conductive mass when substituting part of the carbon black by graphite.

The situation drastically changed when the carbon concentration was decreased as shown in Figs. 15 and 16. At a carbon amount of 3 wt.%, the electrical volume resistivity of the pure graphite containing samples was higher than for the samples containing either one of the C-NERGY™ carbon blacks. Such a low carbon amount for graphite is, presumably due to its higher volume density, close to the critical volume fraction, i.e. near the percolation threshold of the percolation curve. Thus in this concentration range a small variation of the graphite amount causes a large variation of the resistivity, i.e. a small reduction of the graphite amount significantly increases the electrical resistivity of the electrode. Amongst the graphite grades studied, the electrical resistivity of $LiCoO_2$ powder mixture decreased in the order KS6-KS6L-SFG6L according to the decrease of the volume density. In the same order the compressibility of $LiCoO_2$ powder mixture increased. In the low carbon concentration range of the conductive mass, graphite positively affects the compressibility of the $LiCoO_2$ powder mixture and leads to higher sample densities than carbon black.

Another interesting aspect of the C-NERGY™ carbon blacks was observed when studying combinations of carbon black and graphite in the low concentration range of the conductive mass in the $LiCoO_2$ powder mixture. The $LiCoO_2$ powder sample containing, at 3 wt.% total carbon amount, a mixture of one of these carbon blacks and graphite in a weight ratio of 1:1 shows an increased compressibility and only a slight increase of the electrical resistivity. At this low concentration, the graphite and carbon black component in the mixed carbon conductive mass seem to act independently. The graphite component at a netto amount of 1.5 wt.% presumably is below the critical volume fraction whereas the carbon black component still is above. Thus solely carbon black is taking the role as conductivity enhancer which even at low amounts such as 1.5 wt.% delivers a sufficient conductivity to the electrode mass whereas the

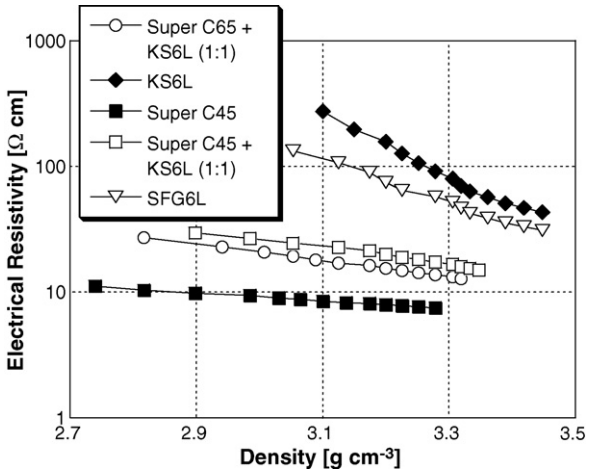

Fig. 16. Electrical resistivity versus sample density of dried powder samples consisting of $LiCoO_2$ and 3 wt.% of total carbon conductive mass mixed in acetone under high shear energy. Conductive additives were C-NERGY™ KS6L and C-NERGY™ SFG6L graphite as well as blends of C-NERGY™ Super C65 and TIMREX® KS6L or C-NERGY™ Super C45 and C-NERGY™ KS6L (1:1 by weight).

graphite component acts as compaction aid which improves the compressibility of the electrode mass to increased press densities.

4. Conclusion

C-NERGY™ Super C45 and C-NERGY™ Super C65 are suitable conductive carbon blacks for electrodes in advanced lithium ion batteries. Both carbon blacks decrease the electrical resistivity of standard $LiCoO_2$ electrodes to a similar level outperforming most of the existing low surface area conductive carbon blacks. However, for optimal results in terms of electrode resistivity, a homogeneous dispersion of carbon black in the electrode mass only can be achieved by adapting the mixing process to the specific properties of each carbon black. The facile dispersibility of C-NERGY™ Super C45 allows even dry-mixing of the carbon black with the positive $LiCoO_2$ electrode material whereas for C-NERGY™ Super C65 dry-mixing does not lead to homogeneous dispersions of the carbon black in the $LiCoO_2$ electrode mass. The difference in dispersibility between the C-NERGY™ carbon blacks can be explained by the surface group chemistry which in the case of C-NERGY™ Super C45 shows a lower degree of graphitization and a higher concentration of hydrogen, oxygen, and carboxylic acid groups. The lower BET SSA of C-NERGY™ Super C45 is the reason for the lower viscosities of solvent or aqueous dispersions of this carbon black. The lower amount of liquid required when preparing the coating dispersion during the electrode manufacturing and as a consequence the shorter electrode drying times are process advantages expected for the application of this carbon black in lithium ion battery electrodes. The principle results obtained for the C-NERGY™ carbon blacks in combination with $LiCoO_2$ presumably could be transferred to alternative electrode materials with similar particle size and shape.

Due to the higher volume density compared to conductive carbon black, the graphite conductive additives TIMREX® KS6, C-NERGY™ KS6L, and C-NERGY™ SFG6L show higher critical volume fractions. At graphite amounts slightly above the critical volume fraction, the electrical resistivity of a graphite containing $LiCoO_2$ electrode decreases in the order KS6 > KS6L > SFG6L which can be explained by their volumetric density decreasing in the same order. With further increasing graphite amounts, the electrical resistivity of the $LiCoO_2$ electrode containing either one of the graphite grades gradually reaches the same level. This ultimate resistivity level is significantly lower for graphite than for conductive carbon black containing electrode masses. One explanation could be the higher compressed densities achieved for graphite containing $LiCoO_2$ electrodes. At higher electrode densities the direct interparticle contacts between the graphite particles (or between particles of graphite and $LiCoO_2$) which form the conductive paths within the electrode mass are improved, hence lowering the electrical resistivity level of the electrode. Higher densities also could decrease the distance between the carbon black aggregates in the mixed carbon conductive mass presumably improving an electron tunneling, hopping, or direct interparticle contact. The addition of graphite to the carbon black conductive mass causes higher densities at given compaction pressures and therefore, at graphite amounts above the critical volume fraction, leads to an improved electrical resistivity of the compressed electrode. Additionally, the higher thermal conductivity of graphite could cause improved heat dissipation in the electrode.

In the case of a carbon conductive mass containing graphite below and carbon black above the critical volume fraction, carbon black maintains the role as conductivity enhancer whereas graphite only acts as compaction aid thus improving the press density of the electrode. Graphite and conductive carbon blacks have complementary roles in the mixed conductive mass at low concentrations. Combinations of graphite and carbon black in the conductive electrode mass therefore increase the degree of freedom for the fine-tuning of the electrode design when optimizing the electrode performance.

References

[1] H. Yang, S. Amiruddin, H.J. Bang, Y.-K. Sun, J. Prakash, J. Ind. Eng. Chem. (Seoul, Republic of Korea) 12 (2006) 12–38.
[2] B. Scrosati, Chem. Rec. 5 (2005) 286–297.
[3] M. Broussely, P. Biensan, F. Bonhomme, P. Blanchard, S. Herreyre, K. Nechev, R.J. Staniewicz, J. Power Sources 146 (2005) 90–96.
[4] M. Broussely, in: G.-A. Nazri, G. Pistoia (Eds.), Lithium Batteries, Kluwer Academic Publishers, Norwell, MA, USA, 2004, pp. 645–685.
[5] C. Fellner, J. Newman, J. Power Sources 85 (2000) 229–236.
[6] Y. Nishi, K. Katayama, J. Shigetomi, H. Horie, 13th Annu. Battery Conf. Appl. Adv., 1998, pp. 31–36.
[7] D. Bechtold, T. Brohm, M. Maul, E. Meissner, Proc. Power Sources Conf., 38th, 1998, pp. 508–511.
[8] U. Koehler, F.J. Kruger, J. Kuempers, M. Maul, E. Niggemann, H.H. Schoenfelder, Proc. Intersoc. Energy Convers. Eng. Conf., 32nd, 1997, pp. 93–98.
[9] R.J. Brodd, K. Tagawa, in: W.A. Van Schalkwijk, B. Scrosati (Eds.), Advances in Lithium-Ion Batteries, Kluwer Academic/Plenum Publishers, New York, USA, 2002, pp. 267–288.
[10] R.J. Brodd, Proc. Electrochem. Soc. 2000 (36) (2001) 14–26.
[11] P. Novák, W. Scheifele, M. Winter, O. Haas, J. Power Sources 68 (1997) 267–270.
[12] O. Haas, E. Deiss, P. Novák, W. Scheifele, A. Tsukada, Proc. Electrochem. Soc. 97 (18) (1997) 451–462.
[13] P. Novák, D. Goers, M.E. Spahr, in: F. Béguin, E. Frackowiak (Eds.), Carbons for Electrochemical Energy Storage and Conversion Systems, CRC Press, Taylor&Francis Group, Boca Raton, FL, 2010, pp. 263–328.
[14] M.E. Spahr, in: M. Yoshio, R.J. Brodd, A. Kozawa (Eds.), Lithium-ion Batteries—Science and Technology, Springer, New York, 2009, pp. 117–154.
[15] Y.B. Yi, C.W. Wang, A.M. Sastry, J. Electrochem. Soc. 151 (2004) A1292–A1300.
[16] Y.B. Yi, L. Berhan, A.M. Sastry, J. Appl. Phys. 96 (2004) 1318–1327.
[17] Y.B. Yi, A.M. Sastry, Phys. Rev. E: Stat., Nonlinear, Soft Matter Phys. 66 (2002) 066130/066131–066130/066138.
[18] Y.-H. Chen, C.-W. Wang, G. Liu, X.-Y. Song, V.S. Battaglia, A.M. Sastry, J. Electrochem. Soc. 154 (2007) A978–A986.
[19] C.W. Wang, K.A. Cook, A.M. Sastry, J. Electrochem. Soc. 150 (2003) A385–A397.
[20] H. Wang, T. Umeno, K. Mizuma, M. Yoshio, J. Power Sources 175 (2008) 886–890.
[21] A. Momchilov, A. Trifonova, B. Banov, B. Pourecheva, A. Kozawa, J. Power Sources 81–82 (1999) 566–570.
[22] N. Probst, in: J.-B. Donnet, R.C. Bansai, M.-J. Wang (Eds.), Carbon Black—Science and Technology, CRC Taylor&Francis/Marcel Dekker, Inc., New York, 1993, pp. 271–288.
[23] S.E. Cheon, C.W. Kwon, D.B. Kim, S.J. Hong, H.T. Kim, S.W. Kim, Electrochim. Acta 46 (2000) 599–605.
[24] G. Kühner, M. Voll, in: J.-B. Donnet, R.C. Bansai, M.-J. Wang (Eds.), Carbon Black—Science and Technology, Marcel Dekker, Inc., New York, 1993, pp. 1–66.
[25] C. Poleunis, X. Van den Eynde, E. Grivei, H. Smet, N. Probst, P. Bertrand, Surf. Interface Anal. 30 (2000) 420–424.
[26] P. Novák, W. Scheifele, F. Joho, O. Haas, J. Electrochem. Soc. 142 (1995) 2544–2550.
[27] W.M. Hess, C.R. Herd, in: J.-B. Donnet, R.C. Bansai, M.-J. Wang (Eds.), Carbon Black—Science and Technology, CRC Taylor&Francis/Marcel Dekker, Inc., New York, 1993, pp. 89–174.
[28] E. Grivei, N. Probst, Kautschuk Gummi Kunststoffe 56 (2003) 460–464.
[29] N. Probst, E. Grivei, Carbon (2002) 201–205.